Rates of sea-level rise are highly sensitive to ice viscosity parameters in model benchmarks

D.F. Martin[1*], S.B. Kachuck[2], M. Trevers[3], J.D. Millstein[4], S.L. Cornford [3], B.M. Minchew[5,6]

[1]Applied Mathematics and Computational Research Division, Lawrence Berkeley National Laboratory, Berkeley, CA, USA
[2]Climate and Space Sciences and Engineering, University of Michigan, Ann Arbor, MI, USA
[3]School of Geographical Sciences, University of Bristol, Bristol, UK
[4]Department of Geophysics, Colorado School of Mines, Golden, CO, USA
[5]Department of Earth, Atmospheric, and Planetary Sciences, Massachusetts Institute of Technology, Cambridge, MA, USA
[6]Seismological Laboratory, California Institute of Technology, Pasadena, CA, USA

Key Points:

- Ice sheet model projections are sensitive to the choice of flow law exponent, which governs how ice viscosity responds to changes in stress.
- Models incorrectly assuming $n = 3$ can be initialized to match $n = 4$ glaciers, but significantly underestimate ice loss in retreat benchmarks.
- This bias increases with the speed of retreat, indicating a need to assess uncertainty from ice rheology mismatches in sea level projections.

*1 Cyclotron Rd, Berkeley, CA 94720, USA

Corresponding author: Dan Martin, `DFMartin@lbl.gov`

Abstract

Glacier flow plays a major role in current and future rates of globally averaged sea-level rise. The viscosity of glacial ice, controlling the rate of flow, decreases as stress increases and is highly sensitive to the value of the stress exponent, n, in the constitutive equation for viscous flow. Glaciologists and climate modelers almost exclusively assume $n = 3$ when modeling ice flow and projecting sea-level rise through forward modeling. However, recent work suggests that $n \approx 4$ better fits observations, prompting the question: How sensitive are projections of sea-level rise to the value of n? We use an established community ice flow model and standard benchmark experiments designed as an idealized representation of Pine Island Glacier, West Antarctica. While initializing an $n = 3$ model to match observations of an $n = 4$ ice sheet is possible, we find that incorrectly assuming $n = 3$ when in fact $n = 4$ dramatically underestimates rates of sea-level rise. The scale of this error grows nonlinearly with the magnitude of the climate forcing, acting to increase projection uncertainties. Additionally, we find that models often account for this stress-dependent rheology mismatch during model initialization in a way that masks this rheological effect in the short term while leaving model outputs vulnerable to larger biases in longer-term projections. Initializations to observations of Pine Island Glacier display similar rheology-mismatch fingerprints to our idealized example.

Plain Language Summary

The ice found in glaciers and ice sheets responds to applied stresses with reduced resistance to flow and deformation: push twice as hard, get more than twice the flow. We can model this behavior with a stress-dependent viscosity whose exponent, n, governs the sensitivity of flow to changes in stress. Recent work suggests that $n = 4$ in many regions, departing from the current standard practice of $n = 3$, a pervasive assumption that underpins all existing sea level projections that depend on modeling the flow of ice sheets. We ask: If numerical ice sheet models have been using incorrect values of n, how does that affect their model projections for ice sheet change? We show that in benchmark models of marine ice sheets typically found in Antarctica, using $n = 3$ when n should be 4 leads to underestimates of 100-year sea-level rise contributions of between 21% and 35% depending on the climate forcing. Our work highlights that a simple quantity prescribed for the physical behavior of ice has far reaching implications for modeling of ice sheets and understanding future sea level rise.

1 Introduction

The present reality of global sea level rise (SLR) will impact hundreds of millions of people globally by 2100 (Kulp & Strauss, 2019; Oppenheimer et al., 2019). The magnitude and timing of SLR risk depends on the dynamic response of ice sheets and glaciers to changes in climate, particularly in response to marine forcing from incursion of warmer water into the cavities under ice shelves. The dynamic response of ice sheets, in turn, depends fundamentally on the viscosity of glacial ice and its response to perturbations within the ice column and in the environment.

The ice found within glaciers and ice sheets deforms as a “shear-thinning” (strain-weakening) non-Newtonian viscous fluid. (Budd & Jacka, 1989) To model this behavior, ice flow is often represented using a power law rheology (J. Glen, 1952). Conventionally, most ice sheet models assume Glen’s Flow Law (J. W. Glen & Perutz, 1955) to describe the relationship between the deviatoric stress tensor τ_{ij} and strain rate tensor $\dot{\varepsilon}_{ij}$:

$$\tau_{ij} = 2\eta\dot{\varepsilon}_{ij} \quad \text{with} \quad \eta = \frac{\tau^{1-n}}{2A_n} \tag{1}$$

where the dynamic viscosity η is a function of $\tau = \sqrt{\tau_{ij}\tau_{ij}/2}$, the square root of the second invariant of the deviatoric stress tensor, and the prefactor $A_n = A_{0,n} \exp -\frac{Q}{RT}$ which is a function of absolute temperature T, the universal gas constant R, and material properties such as activation energy Q and those represented by $A_{0,n}$, which has units of Pa^{-n} a^{-1} (Budd & Jacka, 1989; K. M. Cuffey & Paterson, 2010). The flow law exponent n is taken to be a scalar where different values indicate particular mechanisms of deformation (Goldsby & Kohlstedt, 2001). Laboratory experiments show that the physical mechanisms for ice deformation, and thus the values of A_n and n, vary depending on stress, temperature, and impurity content (Schulson & Duval, 2009; Goldsby & Kohlstedt, 2001). While experimental data suggest a wide variability in the viscous parameters (Bromer & Kingery, 1968; Duval et al., 1983; Goldsby & Kohlstedt, 2001; Steinemann, 1954), ice sheet models have historically assumed $n = 3$ as the standard, and only, value of the flow law exponent (e.g., S. Cornford et al. (2013); Larour et al. (2012); Hoffman et al. (2018); Lipscomb et al. (2019); Gagliardini et al. (2013); Khrulev et al. (2025)).

Recently, however, analysis of observational and in situ data suggests that a higher value of the flow law exponent may better match the behavior of ice flow at scales relevant to the natural world (Bons et al., 2018; K. Cuffey & Kavanaugh, 2011; Gillet-Chaulet et al., 2011; Jezek et al., 1985; Millstein et al., 2022; Fan et al., 2025; Wang et al., 2025). For at least some of the deformation regimes most commonly observed in areas with high strain rates in the Antarctic and Greenland Ice Sheets, these results suggest that $n = 4$ can better represent observations than the canonical $n = 3$. As a specific example, Millstein et al. (2022) infer $n = 4.1 \pm 0.4$ based on observations of ice deformation and thickness in Antarctic ice shelves, with largely unquantified implications for modeling the evolution of ice sheets and their contribution to sea-level rise.

In recent years, the ice sheet modeling community has contributed a number of increasingly sophisticated projections of SLR designed to inform climate scientists and decision-makers (e.g., S. L. Cornford et al. (2015); Seroussi et al. (2020); Edwards et al. (2021); Seroussi et al. (2024)). Since most, if not all, contemporary ice sheet models use flow laws with $n = 3$, this leaves open the question of what implications the higher value of $n = 4$, and resulting nonlinearity, might have on ice sheet model projections and the understanding of ice sheet dynamics that has been gleaned from their use. For example, Getraer and Morlighem (2025) performed a set of experiments based on the ISMIP6 projection experiments (Seroussi et al., 2020) and found that using an $n = 4$ rheology resulted in a 32±14% increase in ice loss from the Amundsen Sea Embayment (ASE), in West Antarctica by 2100 compared with similar projections with $n = 3$ and a roughly $70 \pm 15\%$ increase by 2300. However, in the same region, Sergienko (2025) found a more limited impact, with consequences on ice thickness and speed limited to around 5%. These contested uncertainties in SLR projections arising from an unresolved uncertainty in n motivate this study, where we employ the framework of simple and relevant community model benchmarks to explore the impacts of a higher than typical value of n.

We look to gain understanding of the impacts of incorrectly initializing a model with $n = 3$ to match a spun up ice sheet state with the true value of $n = 4$, and then comparing resulting projections of the behavior of the incorrectly initialized $n = 3$ model against the true $n = 4$ ice sheet. Our approach is motivated by simplicity, where we aim to analyze the discrepancies between $n = 3$ and $n = 4$ projections in a controlled set-up. Our ability to prescribe the true value of n and other relevant parameters, generate synthetic data used to initialize ice-flow models from prescribed (and known) parametric values, and initialize our model with values of n that differ from the true value allows us to isolate and assess how the model results differ between the true model and one that assumes a different value of n. To our knowledge, this is the first study to take this approach. Previous studies by Getraer and Morlighem (2025) and Sergienko (2025) use observations of the Antarctic Ice Sheet, where the value of and uncertainties in n and other relevant physical parameters are not fully constrained, introducing unexplored and unquantified parametric uncertainties into their results that do not exist in our idealized study. In this way, our study complements and expands on the findings of these previous studies by targeting a simple comparison ice flow and different stress responses.

2 Methods

2.1 The Role of Observations in Ice Sheet Modeling

Ice sheet models require spatially-varying parameter fields which are not easily observed, like the coefficient of friction at the beds of glaciers and parameters which represent local deviations from the standard Glen's Law due to local physical processes like damage, ice fabric and grain size, strain-induced heating and other localized and transient thermal effects, interstitial liquid water content, and impurities. To address this when simulating present-day ice sheets, ice sheet modelers commonly create initial conditions for their experiments to match (as best as possible) observations of existing ice sheets. The observations include basal topography, surface elevation, and ice velocities. In ice sheet models, the ice velocities are obtained by solving a system of nonlinear partial differential equations derived from the momentum balance. Many, if not most, ice sheet modelers reproduce a fit to observed velocities for a given ice geometry by inferring values for the (harder to measure) basal friction coefficient and some combination of viscous parameters, such as $A_{0,n}$ or T. (MacAyeal, 1993; Morlighem & Goldberg, 2023)

In this study, we use the BISICLES model (S. Cornford et al., 2013), and infer a basal friction field along with a viscosity multiplier coefficient ϕ (sometimes called an"enhancement factor" (Minchew et al., 2018)) as a proxy for the effects on ice viscosity of mismatches between expected and actual damage, temperature fields, fabric, impurities, and liquid water content (S. L. Cornford et al., 2015). As the name suggests, ϕ multiplies the viscosity in Equation 1, which then becomes

$$\tau_{ij} = 2\phi\eta\dot{\varepsilon}_{ij}. \tag{2}$$

While modelers generally assume that their models broadly represent the physics of glacial ice, we note that this approach does not actually require that the rheology assumed in the model be a particularly good representation of the physics of the observed ice. John von Neumann would say, "Give me four parameters and I can fit an elephant; with five I can make him wiggle his trunk"; given the number of parameters and nonuniqueness in both the spatially varying basal friction and viscosity multiplier fields, there are presumably many combinations which allow one to fit a model that assumes $n = 3$ in Equation 1 to observations of an ice sheet regardless of the physical processes at work (MacAyeal, 1993; Gudmundsson, 2003; Dyson, 2004) .

It is not yet possible to infer the values of A and n in grounded areas where the friction at the bed is unknown due to limitations in our observations and the uncertainties in the inferences of the friction coefficient at the bed. As a result, while the process of tuning basal friction and ice viscosity parameters to fit observations is effective in initializing models to modern observations, it can create uncertainties in time-dependent evolution of models because constitutive parameters like n govern modeled ice sheet evolution. To illustrate this point, consider that studies which infer the basal friction coefficient and the value of $A_{0,3}$ (assuming $n = 3$) show that values of $A_{0,3}$ tend to be larger in areas of rapid shear and deformation [e.g., (Ranganathan, Minchew, Meyer, & Gudmundsson, 2021)]. The higher value of $A_{0,3}$ in these areas relative to the surrounding areas indicates localized deformation, which is often attributed to a combination of crystallographic fabric development and grain size evolution, local variations in ice temperature, and damage (Hudleston, 2015; Minchew et al., 2018). However, increasing n from 3 to 4 is likely to further localize deformation in ice sheets (Turcotte & Schubert, 2014).

For initializations or short-term projections, this distinction in physical mechanisms may not be important, but when evolving the model over long periods of time, it has the potential to lead to different results because the value of n, the development of fabric, local shear heating, and the damage development lead to different rates and magnitudes of change in viscosity.

2.2 The MISMIP+ and ABUMIP Ice Sheet Model Benchmarks

To explore the ice-sheet-modeling consequences of errors in n, we use the MISMIP+ benchmark (Asay-Davis et al., 2016; S. L. Cornford et al., 2020), which is designed to explore the impact of ice shelf thinning (and resulting weakening of buttressing effects) in marine ice sheets, currently believed to be a primary driver of Antarctic contributions to SLR in the present day and for the next century. The ice sheet configuration (Figure 1) is a glacier in a trough with a section of retrograde bed. The basal friction and surface mass balance are tuned to place the steady-state grounding line on the section of retrograde slope indicating a balance between the various competing physics and tendencies present. This steady-state configuration is then perturbed by introducing a depth-dependent subshelf melt-rate, resulting in ice shelf thinning and weakening, reducing buttressing (the back-stress ice shelves exert on the upstream ice), which in turn results in upstream acceleration, thinning, and grounding-line retreat. The configuration represents a simplified Pine Island Glacier, and is designed to explore the impact on marine ice sheet systems of buttressing and ice-shelf weakening due to warm-water incursion as has been observed in the Amundsen Sea Embayment in West Antarctica, where Pine Island Glacier resides. A similar modeling benchmark, the ABUMIP experiments (Sun et al., 2020), applies an extreme melt forcing to any floating ice, rapidly eliminating ice shelves. This provides an indication of the maximum possible response to rapid ice shelf loss or collapse, and can be an indication of marine ice sheet vulnerability (Martin et al., 2019).

In this work, we use the MISMIP+ and ABUMIP benchmark experiments to explore the consequences of initializing an ice sheet model which assumes $n = 3$ to observations of a marine ice sheet in which $n = 4$. We do this by first generating an ice-sheet state with an underlying rheology using $n = 4$, then initializing our $n = 3$ model to match our synthetically “observed” thickness and velocity field following S. L. Cornford et al. (2015). We then perform evolution experiments forced by specified sub-shelf melting profiles to observe how the $n = 3$ model differs from the true $n = 4$ behavior. Using this idealized set up allows us to isolate precisely the consequences of assuming a particular flow-law exponent on initializing and projecting the grounding line evolution of an embayed ice shelf that buttresses a grounded glacier, like Pine Island, without the compounding and trading-off uncertainties of basal friction or other mechanisms that complicate searching for an initial state. By including the ABUMIP benchmark experiment we furthermore explore a proxy for ice shelf collapse that hasn’t been considered in previous work on the impact of n on the response to ice sheets to ocean-induced melting (Getraer & Morlighem, 2025; Sergienko, 2025).

2.3 Ice Sheet Model

Our numerical experiments employ the BISICLES model (S. Cornford et al., 2013), which uses a variant of the vertically-integrated “L1L2” stress balance (Schoof & Hindmarsh, 2010). BISICLES employs adaptive mesh refinement to ensure that fine mesh resolution is dynamically deployed as needed; for these experiments, mesh resolution ranges from a coarsest resolution of 4 km in quiescent regions down to a finest resolution of 250 m near grounding lines and regions of high strain rates. We use the Coulomb-limited basal friction rule from Tsai et al. (2015).

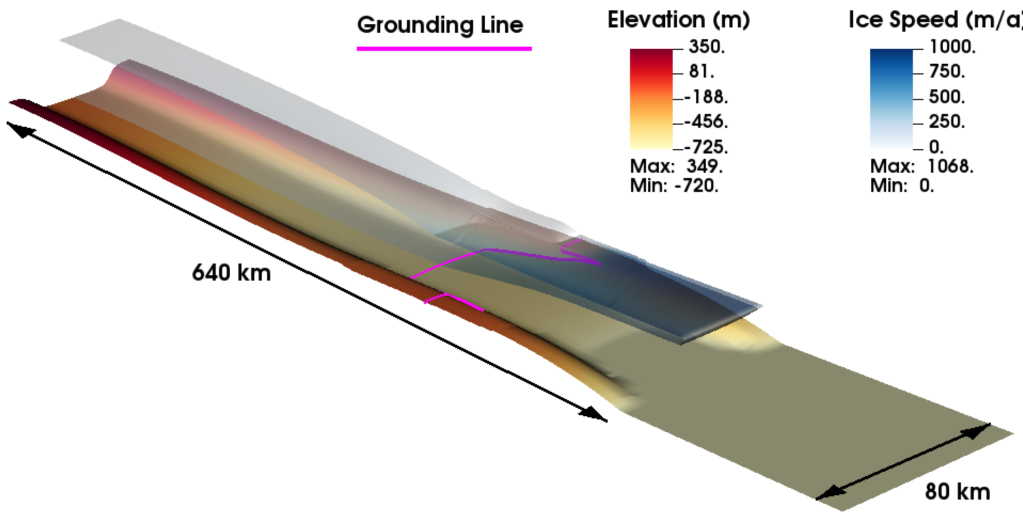

Figure 1. Schematic of the initial conditions for the model experiments in this work. The glacier flows from upper left to lower right in a trough. Upper and lower ice surfaces are painted with ice speed (darker blue is faster-flowing ice). Ice is cut away at the centerline to reveal bedrock topography (orange/brown coloring). The grounding line (where the ice transitions from grounded to floating) is depicted by a magenta line. Note that the vertical dimension has been stretched by 20x for clarity. More details in Asay-Davis et al. (2016).

2.4 MISMIP+ Spinup and Choosing a value for A_n

The MISMIP+ experiment begins with a constant-temperature ice sheet, on a bed with a constant basal-friction coefficient C and ϕ equal to unity, spun up to a steady-state configuration without any subshelf melt forcing and with a constant surface accumulation rate. The upstream boundary is taken to be an ice divide, and the lateral boundaries are free-slip. We choose values of A and the basal friction coefficient so that a spun-up steady-state ice sheet places its grounding line on the retrograde bed at the centerline of the domain.

For this experiment, we use the values of the basal friction coefficient C and accumulation rate $\dot{a}$ suggested by Asay-Davis et al. ($C = 1{\times}10^4$ Pa m$^{\frac{1}{3}}$ a$^{-\frac{1}{3}}$, $\dot{a} = 3$ m a^{-1}) and then choose the value of A by running an ensemble of spin-up experiments to find one in which the steady-state grounding line at the centerline of the domain is on the retrograde slope (near $x = 550$ km) per the MISMIP+ problem specification (Asay-Davis et al., 2016). In the $n = 4$ case, we found that a spatially constant value of $A_4 = 1.9\times 10^{-22}$ Pa^{-4}a^{-1} (6.02×10^{-30} Pa^{-4}s^{-1}) worked well. Following the approach outlined in the Appendix, we calculate $A_3 = A_4\tau_{ref} = 1.71{\times}10^{-17}$ Pa^{-3}a^{-1} ($5.46{\times}10^{-25}$ Pa^{-3}s^{-1}) for $\tau_{ref} = 90$ kPa. This value of A_3 is comparable to the suggested value of $2.0{\times}10^{-17}$ Pa^{-3}a^{-1} from Asay-Davis et al. (2016). We define the reference stress $\tau_{ref} = 90$ kPa because it produced a ϕ distribution that is roughly symmetric and centered on the reference value $\phi = 1.0$. We note, however, that because the MISMIP+ experiment is a constant-temperature ice sheet, our assumption for the value of τ_{ref} merely appears as a spatially constant prefactor to the viscosity, and will be compensated for when we compute ϕ during the inversion process. We tested this by confirming that changing τ_{ref} did not result in a different initial viscosity.

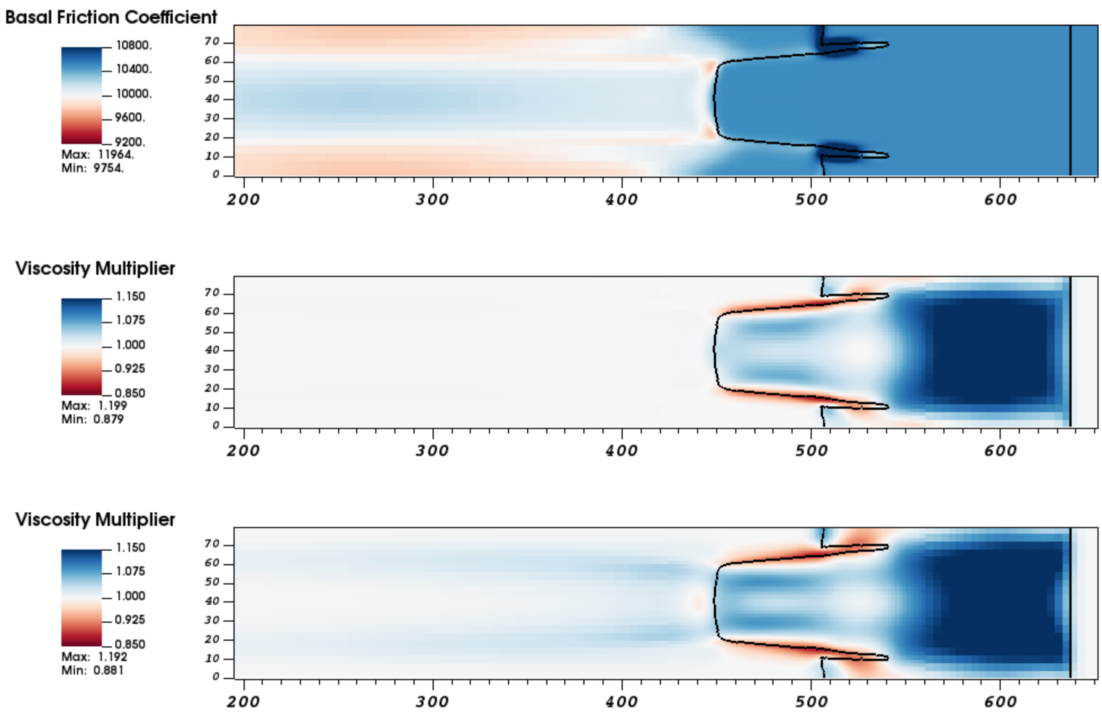

Figure 2. (top) Basal friction coefficient C and (middle) viscosity multiplier, ϕ, computed by $n = 3$ inversion to match $n = 4$ steady-state using a combined inversion for C and ϕ. Black contour indicates grounding-line location, where the ice transitions from grounded into the floating ice shelf. (bottom) Viscosity multiplier computed by $n = 3$ inversion which only inferred ϕ. In the plot of C, red hues indicate lower friction, while blue indicates higher friction coefficients. Note that the colormaps are centered around the prescribed $n = 4$ values of $C = 1.0 \times 10^4\ m^{\frac{1}{3}} a^{-\frac{1}{3}}$ and $\phi = 1.0$. In plots of ϕ, red hues indicate viscosity reduction ("softening"), while blue indicates viscosity increase ("hardening").

2.5 Inversion with $n = 3$

Once we obtained steady-state $n = 4$ MISMIP+ thickness and velocity fields and a matched $n = 3$ value for the rate-factor A_3, we initialized the $n = 3$ model using the approach described by S. L. Cornford et al. (2015) to infer spatially-varying basal friction coefficient (C) and viscosity multiplier (ϕ) fields. Many, if not most, models perform initializations by inferring some combination of the basal friction field under grounded ice along with a viscosity multiplier which usually is primarily active in the floating ice shelves. Details of our inversion approach are described in the supplementary information. The basal friction (C) and viscosity multiplier (ϕ) fields we computed are shown in Figure 2. Note that our inversion attempts to compensate for the rheology mismatch via small-magnitude (on the order of 1 percent) variations in the basal friction field, along with a more-pronounced correction evident in the ϕ field. Since we expect rheology mismatches to be better addressed via the viscosity multiplier, we can also leverage our prior knowledge of the correct value of C in the MISMIP+ problem specification and optimize for the viscosity multiplier ϕ in isolation with C held fixed at the prescribed value; we expect that this approach will lead to a more-faithful representation of the correction needed to match $n = 3$ ice to true $n = 4$ ice. The resulting ϕ field produced by this second inversion is also shown in Figure 2. Whether inverting for basal friction or not, to match the $n = 3$ model to the $n = 4$ synthetic observation requires viscosity reductions in regions of high strain rates (red hues in ϕ in Figure 2), and a corresponding increase in the viscosity in regions of low strain rates (blue hues). In short, we expect the magnitude of variations from $\phi = 1$ to increase with $n = 3$. This is the expected consequence of the increased sensitivity to changes in viscosity with $n = 4$, hence larger perturbations of ϕ are required with $n = 3$ to produce the equivalent effect on ice flow. The primary impact of including the basal friction coefficient in the inversion is in the grounded ice, with little impact on the viscosity multiplier on floating sections or at the grounding line.

2.6 Evolution experiment

With the $n = 3$ rheology initialized to the $n = 4$ initial state via inversion, we carry out a set of experiments for each rheology – a control experiment to confirm steady state and a pair of retreat-and-advance experiments. For the control experiments, we simply restarted the configurations without any additional forcing. For the retreat and readvance experiment, we apply a prescribed subshelf depth-dependent basal melt rate to represent the impact of climate forcing. Starting with the spun-up ice configuration, we allow the ice sheet to retreat under the influence of melt for 100 years, after which we turn off the melt and the ice sheet is allowed to recover, running out a total of 400 years. We perform an additional control run of the $n = 3$ rheology without the inversion-computed viscosity multiplier field to identify the impact of the inversion. For the forced experiments, we use two distinct forcing regimes. *Moderate* forcing uses the depth-dependent melt formula prescribed in the original MISMIP+ experiment (Asay-Davis et al., 2016), which represents currently-observed melt-forcing and shelf-thinning regimes, likely due to incursions of subshelf warm water. A second *extreme* forcing is based on the ABUMIP experiments (Sun et al., 2020) and is designed to represent extreme shelf loss and collapse, like the collapse of the Larsen B Ice Shelf in 2002 (Scambos et al., 2004). The experiments are tabulated in Table 1. Except where specifically indicated, we choose to use the viscosity multiplier inverted with the (known) basal friction parameter rather than the combined inversion to focus on the effects of the viscosity multiplier.

Table 1. Ice sheet experiments performed

Experiment Number	Experiment Name	n	Melt Forcing	ϕ
1	n4Control	4	none	1.0
2	n4MISMIP	4	moderate	1.0
2a	n4ABUMIP	4	extreme	1.0
3	n3Control	3	none	inversion
4	n3Control-no ϕ	3	none	1.0
5	n3MISMIP	3	moderate	inversion
5a	n3ABUMIP	3	extreme	inversion
6	n3MISMIP-combined	3	moderate	combined inversion
6a	n3ABUMIP-combined	3	extreme	combined inversion

3 Experiment Results

3.1 Moderate Melt Experiments

Figure 3 shows snapshots of the evolution of ice velocity, grounding line position and upper ice surface elevation for the $n = 3$ (ϕ-only inversion) and $n = 4$ moderate melt experiments (Experiments 2 and 5 in Table 1). Figure 4 shows the evolution of the grounded area (which is the sum of the ice sheet grounding line advance or retreat) and the change in the total volume of ice above the flotation point (which corresponds to the contribution to SLR in the absence of solid-earth and variable sea-level effects) for the experiments in Table 1. The control runs maintain the initial condition, as expected for a successful (and successfully inverted) steady-state, while the experiment runs initially exhibit the expected thinning, grounding-line retreat, and reduction in volume above flotation (corresponding to a positive contribution to SLR). When the melt forcing is turned off after 100 years in the experiment runs, the ice sheet recovers, albeit at a slower rate than the retreat.

Notable observations from the results:

1. The steady-state configuration is well-maintained in both the $n = 3$ and $n = 4$ control runs (Figure 4, Experiments 1 and 3). This points to the effectiveness of the inversion-produced ϕ field in enabling the $n = 3$ ice sheet to match the initial steady-state $n = 4$ configuration.
2. The $n = 3$ control run with $\phi = 1$ (Experiment 4) experiences a small advance and mass gain (Figure 4). This is a consequence of the $n = 3$ rheology's increased viscosity and decreased sensitivity to changes in shear stress across the ice shelf margin, allowing for a greater buttressing back-stress and the observed thickening and grounding line advance. This demonstrates the impact of the ϕ field when matching observations, and shows that it is relatively straightforward to match an $n = 3$ ice sheet to a snapshot of observations of an $n = 4$ ice sheet using a viscosity multiplier.
3. Owing to its decreased sensitivity to changes in stress and higher initial viscosity, the $n = 3$ ice sheet in Experiment 5 noticeably under-predicts the initial response of the ice sheet relative to the $n = 4$ baseline in Experiment 2, with maximum reduction in grounded area 17.6% less than the $n = 4$ response, and a corresponding 21% underestimate in the reduction in the volume above flotation (contribution to SLR). These results are consistent with modeled projections of Antarctica's contribution to sea level rise as shown in Figure 1B of Fricker et al. (2025). During retreat, when the ice shelf is thinned, the $n = 4$ rheology has a much faster

response time and allows faster draining of grounded ice than predicted with $n = 3$ Figures 3– 5.

4. Conversely, in the recovery phase we see a faster response with $n = 4$, but while the $n = 3$ and $n = 4$ grounding lines have recovered similarly by $t = 400$ years, the ice thickness (as expressed in the volume above flotation) has not recovered to the same degree – it is noticeable in Figure 3 that while the grounding lines for both cases are essentially identical, the ice thickness and velocity fields are noticeably different.
5. Compared to differences with the $n = 4$ evolutions, differences between the $n = 3$ results using the two inversion approaches are relatively small, suggesting these observations are robust regardless of the specific inversion approach used.

We can highlight the differences in response rates between the $n = 3$ and $n = 4$ ice sheets (Experiments 2 and 5) by plotting the relative difference (in percent) between the $n = 3$ and $n = 4$ grounded areas and total volumes above flotation, as in Figure 5. Again, notable features are that the $n = 3$ case underestimates the rates of both retreat and readvance, and that the grounded area (grounding-line location) recovers much more quickly than the ice volume.

3.2 Effect of Ice Shelf Collapse and Loss

Using the same MISMIP+ initial condition and inversion as before, we exposed the ice shelves to the extreme melt forcing (ABUMIP) specified in Sun et al. (2020), essentially removing any floating ice in a very short interval.

The resulting evolution of glacier flow, surface elevation, and grounding line position (Figure 6) along with total grounded area and volume above flotation (Figure 4) broadly follow the same patterns as for the moderate-melt case. Under extreme melt conditions, the less-sensitive $n = 3$ ice sheet retreats an additional $1.44\times$ the grounded area loss and sees a $1.64\times$ reduction in volume above flotation compared to the moderate melt case. The more-sensitive $n = 4$ ice sheet sees a difference of $1.59\times$ in grounded area loss. The response in total volume over flotation is also stark, contributing to global SLR at $1.86\times$ the amount from the moderate-melt experiment. This represents an under-estimate of SLR by the $n = 3$ model of 35% after 100 years. Note that the discrepancy between the $n = 3$ and $n = 4$ response is more than proportionally larger (the ABUMIP response divided by the MISMIP response is greater for $n = 4$ than for $n = 3$). Figure 7 shows the relative response ($\frac{\Delta(VaF)_{ABUMIP}}{\Delta(VaF)_{MISMIP}}$) indicating a larger sensitivity of the $n = 4$ ice to extreme forcing relative to projections from the $n = 3$ model. This discrepancy in sensitivity is particularly pronounced in the initial dynamic phase of the experiments, in which the $n = 4$ ice sheet is as much as 50% more sensitive (defined by the ratio of the ratios) to the more-extreme forcing. However, even in the long-term response, the $n = 4$ sensitivity is 20% more than seen in the $n = 3$ result.

Movies corresponding to Figures 3 and 6 are included in the supplementary material.

4 Application to Pine Island Glacier

It is notable that the pattern our inversion retrieves in the viscosity multiplier closely resembles the patterns that previous studies have tended to produce when attempting to match observed Antarctic velocity fields with $n = 3$ models (e.g., S. L. Cornford et al. (2015)). This pattern, characterized by sharply localized softening in shear margins and diffuse hardening in regions of lower strain rates, can be observed in the upper-left panel in Figure 8, which shows a viscosity multiplier field inverted to reproduce 2010 velocities for Pine Island Glacier, which flows into the Amundsen Sea Embayment in West Antarctica. Bedrock elevation and ice thickness were provided by BedMachine Antarc-

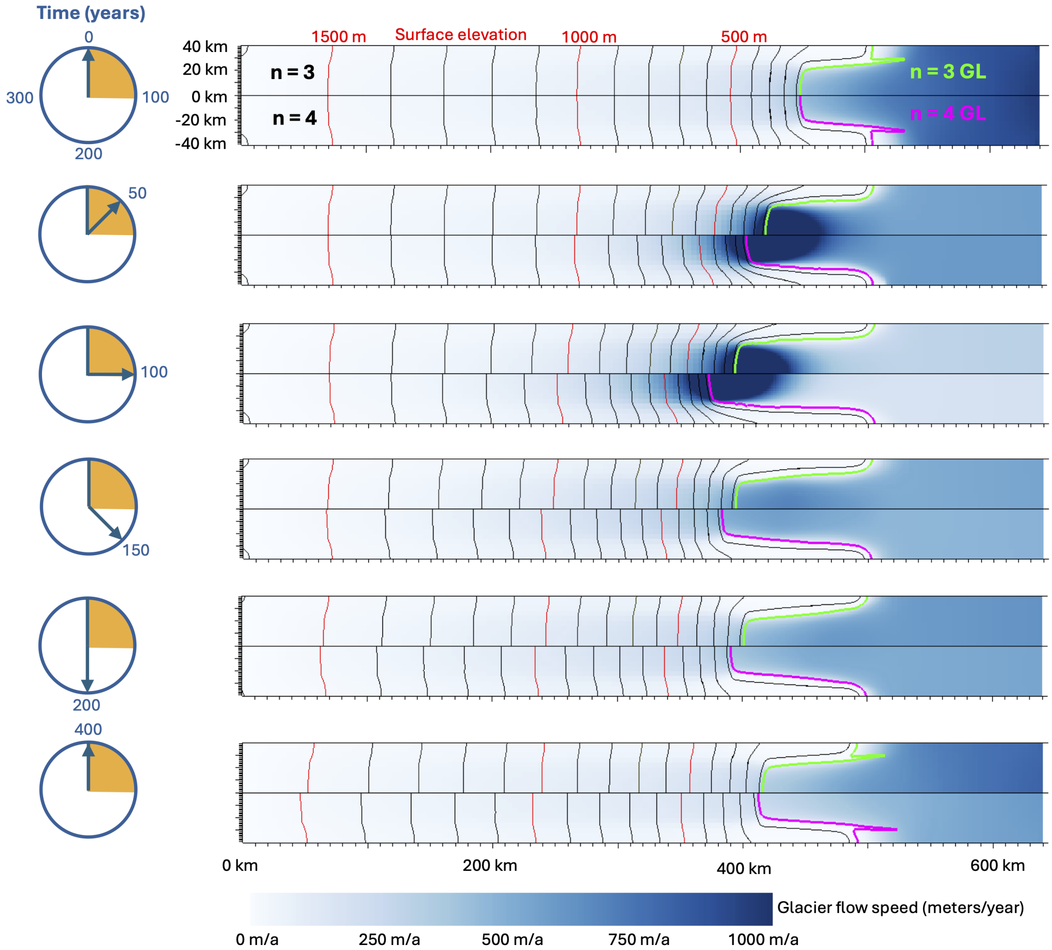

Figure 3. Snapshots of the MISMIP+ (moderate ice-shelf melt) experiment for (from top to bottom) t = 0, 50 years, 100 years, 150 years, 200 years, and 400 years. Glacier flow is from left to right, flow speed is shown in the colormap, thick green and magenta colored lines indicate grounding line position, and red/black contour lines illustrate the upper ice surface elevation. The domain is split – the lower half is $n = 4$ (Experiment 2), and the upper half is $n = 3$ with inversion-produced viscosity multiplier to match initial $n = 4$ velocities at $t = 0$ (Experiment 5). The yellow colored portions of the model time clocks indicate the period 0-100 years when melting is applied to the model, while the remaining time allows the model to recover with no applied melting.

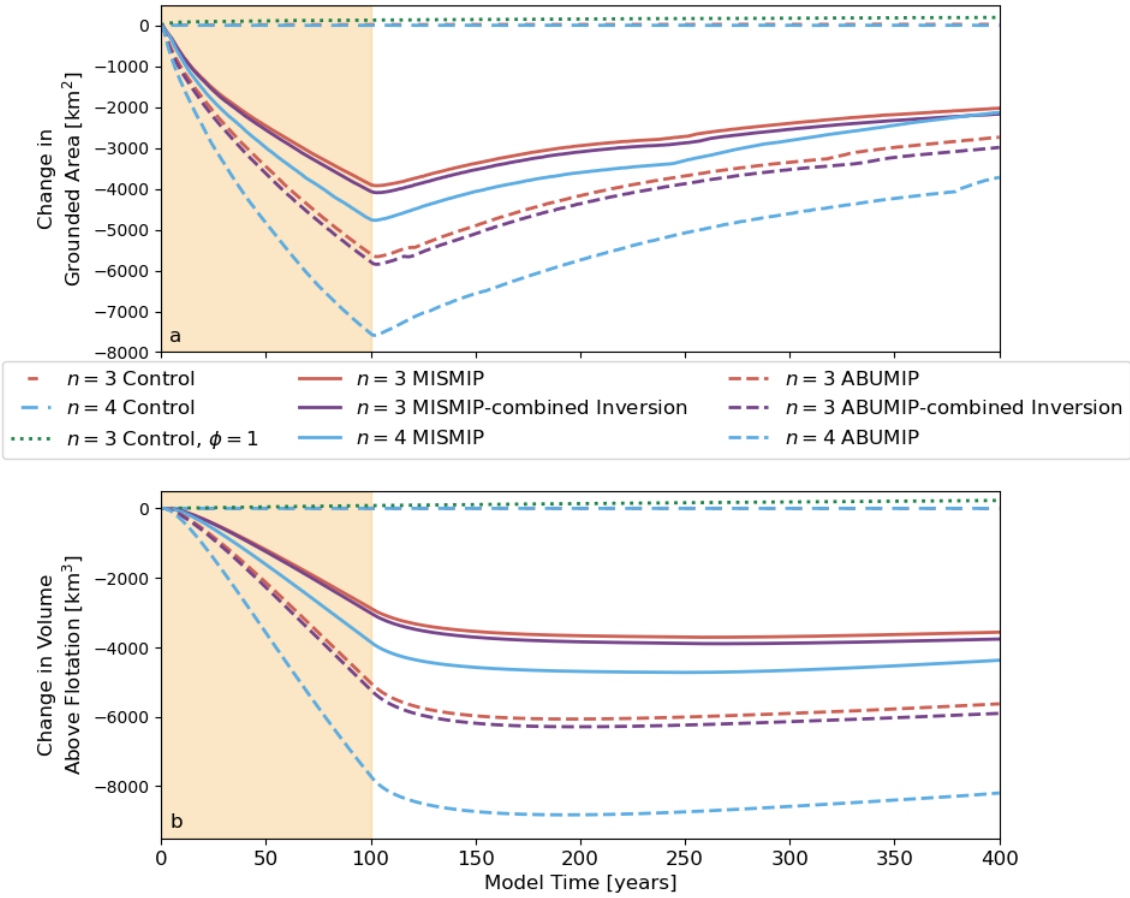

Figure 4. Plots of (top) change in grounded area, and (bottom) change in total volume above flotation for the set of experiments in Table 1. Red indicates $n = 3$ results, purple indicates $n = 3$ results using the combined inversion, green indicates $n = 3$ results holding $\phi = 1$, and blue indicates $n = 4$ results. The yellow shaded region shows the interval of active melt forcing ($t = 0$ to 100 years). Line types denote the specific experiments: control runs (Experiments 1, 3, and 4) are represented by dot-dashed lines, the standard MISMIP+ experiments (Experiments 2 and 5) by solid lines, and the ABUMIP extreme-melt Experiments (2a and 5a) by dashed lines. Note that the lines for $n = 4$ control (Experiment 1) and $n = 3$ control with the inversion-computed ϕ (Experiment 3) overlie and are indistinguishable in these plots.

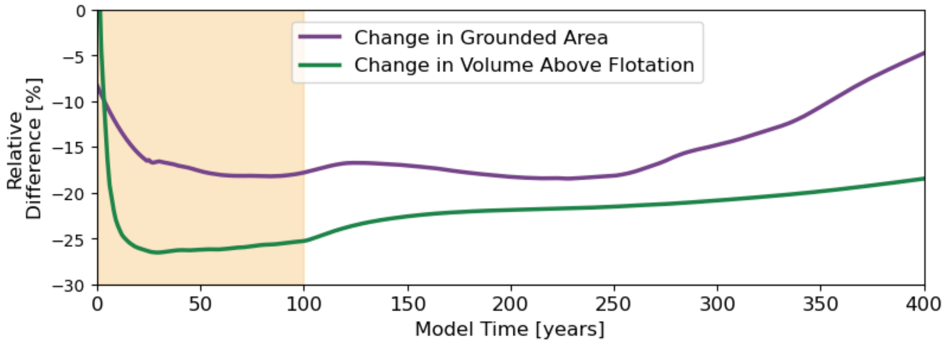

Figure 5. Relative percentage differences in grounded area change and total volume above flotation change between $n = 3$ and $n = 4$ results for Experiments 2 and 5 in Table 1. Relative difference in a time-dependent quantity $Q(t)$ is defined as $(\frac{\Delta Q(t)_{n=3} - \Delta Q(t)_{n=4}}{\Delta Q(t)_{n=4}} \times 100\%)$, in which $\Delta Q(t) = Q(t) - Q(0)$. The yellow shaded region shows the interval of active melt forcing ($t = 0$ to 100 years). Note that the relative difference at the initial time is defined to be zero; as a ratio of two very small numbers at early times, relative differences can change very rapidly causing the initial relative difference of grounded area to appear nonzero on this plot.

tica v3 (Morlighem, 2022), and velocity observations came from Mouginot et al. (2019). Details of the ASE inversions can be found in Supplementary Section S4. In this figure, green hues indicate required increases to the viscosity and purple hues indicate required softening. As with Figure 2, stiffening is required in the main trunks of the ice shelf, along with softening in the shear margins. In the context of this work, the similarities suggest that at least some of the computed viscosity modifications may result from employing an $n = 3$ rheology in the inversion in regions where a different power-law better represents the actual flow of ice.

If this is the case, then one could expect the level of correction imparted by the viscosity multiplier to be less when using an $n = 4$ rheology compared to the standard $n = 3$ rheology. We performed $n = 3$ and $n = 4$ inversions based on ASE observations compiled in Morlighem (2022). Figure 8 shows ϕ for the Pine Island Glacier Ice shelf, computed via $n = 3$ and $n = 4$ inversions, and a representative cross-section across the shelf. In this figure, it is apparent that the $n = 4$ inversions infer noticeably less weakening (about 10% less) in the shear margins, as expected based on our idealized experiment. We also compute the difference between the $n = 3$ and $n = 4$ viscosity multipliers (shown in the middle-left panel in Figure 8). Since $\phi = 1$ in our idealized $n = 4$ ice sheet, this difference is roughly equivalent to the deviation $(\phi - 1)$ in the viscosity multiplier shown in Figure 2. Red regions represent reduced viscosity (weakening), and blue indicates increased viscosity (hardening) for the $n = 3$ inversion relative to the $n = 4$ inversion. We see the same basic pattern as we see in Figure 2 – additional weakening in the ice stream margins for $n = 3$ compared to $n = 4$, and some additional strengthening (blue) in the lower-stress regions in the ice-stream trunks.

Figure 8 also shows the distribution of the viscosity multiplier ϕ within the Pine Island Glacier subdomain (bottom-right panel). Based on the results of our idealized experiment, we expect ϕ to impose less of a correction for the $n = 4$ case than for the $n = 3$ inversion, which is what we see in the figure – the distribution of $\phi_{n=4}$ is more closely clustered around 1 (less corrective) than that for $\phi_{n=3}$. That is consistent with a view that the inclusion of $n = 4$ processes such as dislocation creep better fits the true picture, but also consistent with a view that processes such as fabric formation can emulate higher n in kilometer-scale observations of strain rates.

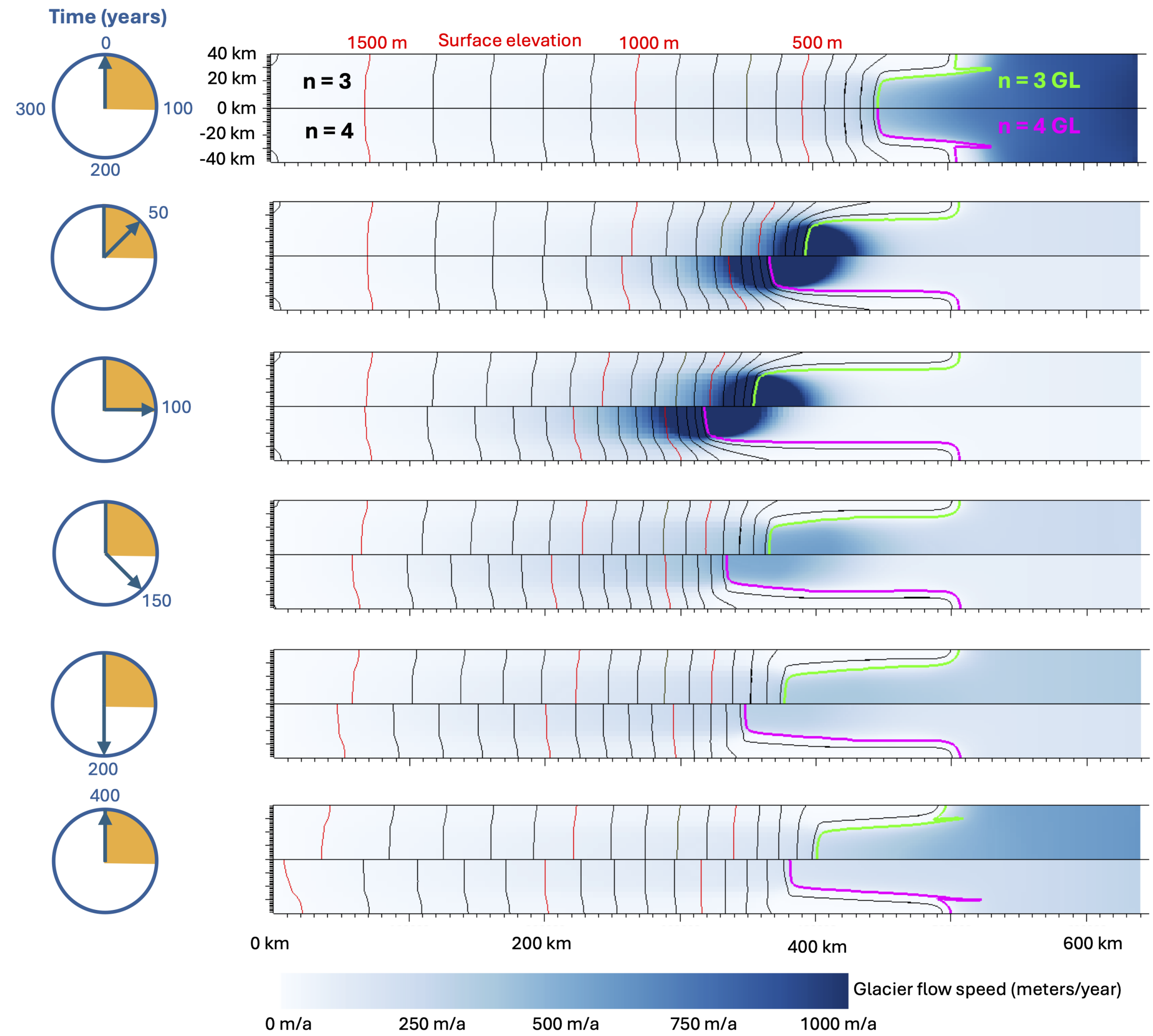

Figure 6. Snapshots of the ABUMIP (extreme melt representing ice-shelf collapse) experiment for (from top to bottom) t = 0, 50 years, 100 years, 150 years, 200 years, and 400 years. Glacier flow is from left to right, flow speed is shown in the colormap, thick green and magenta colored lines indicate grounding line position, and red/black contour lines illustrate the upper ice surface elevation. The domain is split – the lower half is $n = 4$ (Experiment 2a), and the upper half is $n = 3$ with inversion-produced viscosity multiplier to match initial $n = 4$ velocities at $t = 0$ (Experiment 5a). The yellow colored portions of the model time clocks indicate the period 0-100 years when melting is applied to the ice shelf, while the remaining time allows the model to recover with no applied melting.

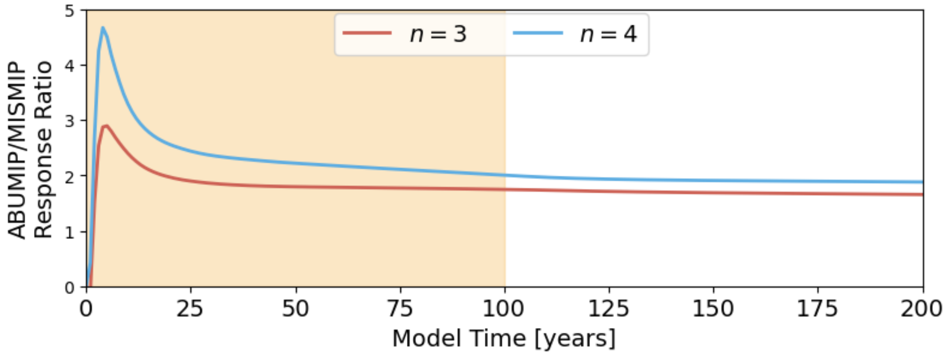

Figure 7. Ratio of change in VaF (contribution to SLR) for the ABUMIP experiment to the change in VaF for the MISMIP+ experiment ($\frac{\Delta(VaF)_{ABUMIP}}{\Delta(VaF)_{MISMIP}}$) for $n = 3$ and $n = 4$.

5 Discussion

All ice-sheet model initializations require modelers to make assumptions and decisions about which parameters to prescribe and which to infer by minimizing the misfit between the model and observations. The results of these inversions can be used to glean insights into the physical mechanisms acting in the ice sheets. For example, some inferred viscosity multiplier (ϕ) values have been interpreted as damage in ice, which naturally tend to occur in regions of high strain rate (C. P. Borstad et al., 2012; Bassis et al., 2024) while others working in different areas of Antarctica highlight the importance of fabric development, recrystallization, and internal shear heating and melting on ice viscosity (Minchew et al., 2018; Ranganathan, Minchew, Meyer, & Gudmundsson, 2021; Ranganathan, Minchew, Meyer, & Peč, 2021). For compactness, we take "softening" to refer to the combined effects of such local deviations from Glen's Law as crevassing, microscopic cracking, warmer ice temperatures, interstitial water, recrystallization, and fabric. The inversion results presented here suggest that at least part of what has been attributed to damage and other softening processes may be the effect of matching an $n = 3$ model to observations of an $n = 4$ ice sheet. If true, this misattribution of physics can have profound impacts on modeling efforts. For example, many efforts are underway to incorporate the physics of ice damage into ice sheet modeling efforts (C. Borstad et al., 2016; Kachuck et al., 2022) – any attempts to validate these models using observations will be complicated by the presence of the effects of rheology mismatches. At the level of this study, there is the parallel case where the true value of n for pure ice is indeed 3, but the softening processes captured by the viscosity multiplier act to cause ice in real-world situations like the ASE to appear as $n = 4$ in data snapshots and short time-series. We note in this case, however, that until robust and well-tested approaches to evolve ϕ fields are developed along with longer data time-series that allow us to distinguish values of n from other softening processes, it is likely that $n = 4$ would remain a better choice for modelers of large-scale marine ice sheets. Regardless, our results, combined with those of Getraer and Morlighem (2025), show that reliable ensemble projections of ice sheet response and resulting contributions to sea level rise must include an exploration of the known uncertainties in the viscous stress exponent n.

In both the MISMIP+ and ASE examples, we are able to match the initial and true $n = 4$ thickness and velocity observations with $n = 3$ using a spatially varying ϕ. But our model's ability to evolve this field is rudimentary at best, and our initialization does not reflect the transient nature of a real ice sheet. It is common practice to simply maintain this spatially-varying ϕ field as constant in time, as we do in our experiments. This means that as the ice sheet evolves, the prescribed viscosity modifications will no longer

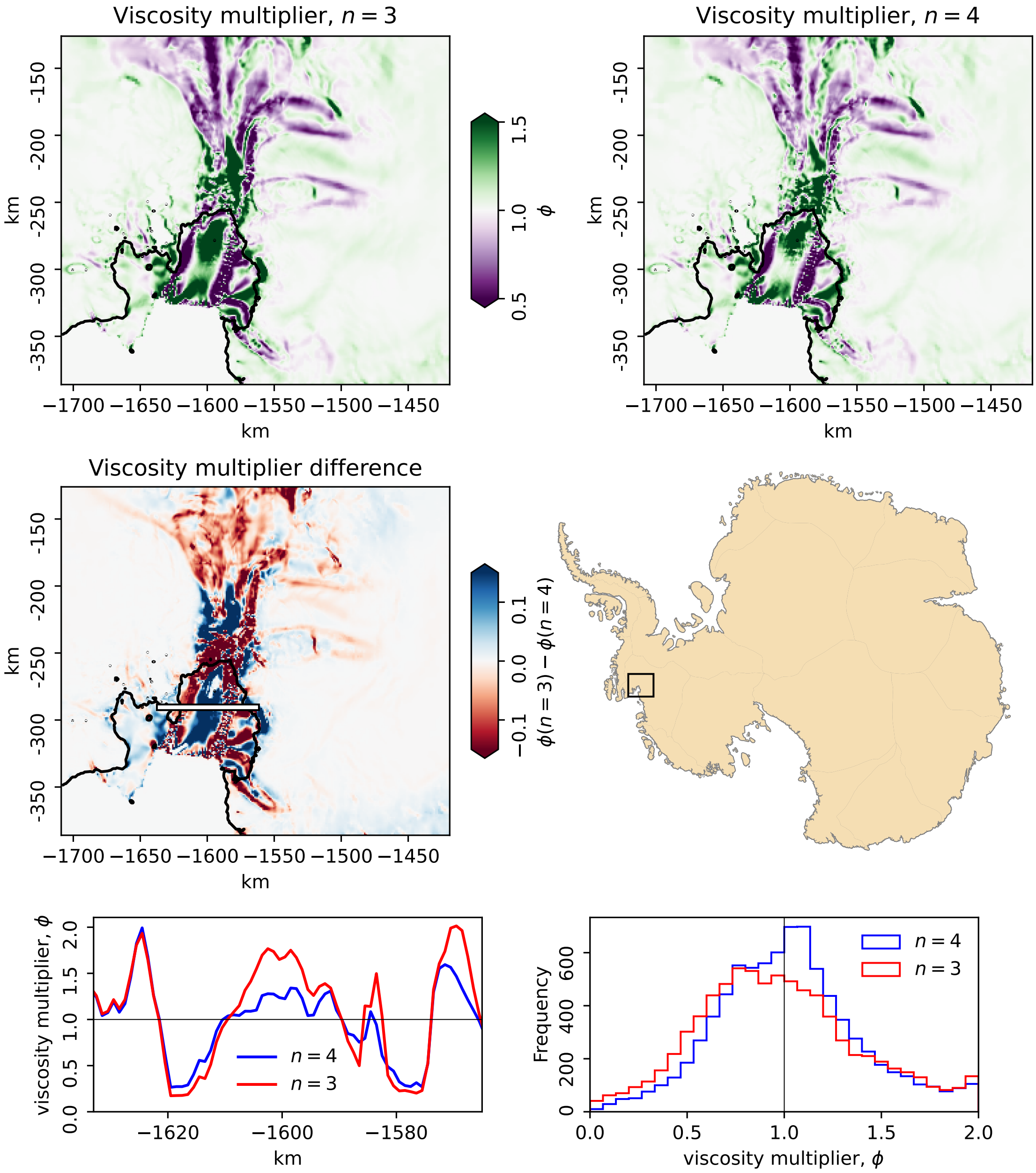

Figure 8. Viscosity multiplier ϕ computed for Pine Island Glacier, West Antarctica, as a part of (top left) $n = 3$ and (top right) $n = 4$ inversions. Green indicates $\phi < 1$ (reduced viscosity) and purple $\phi > 1$ (increased viscosity) (middle left). Difference plot showing $\phi_{n=3} - \phi_{n=4}$. Red denotes viscosity reduction ("softening") for $n = 3$, while blue denotes viscosity increase ("hardening") for $n = 3$ relative to $n = 4$. (middle right) Location of the Pine Island Glacier in West Antarctica, where the map shows only the grounded portions of the ice sheet. (bottom left) Cross-sectional profiles of ϕ along the marked line in (a) and (b). (bottom right) Binned distributions for the inversion parameter ϕ computed in the $n = 3$ and $n = 4$ inversions for Pine Island Glacier, calculated for cells where the ice velocity is in excess of 500 m a^{-1}.

align with current stress fields in the ice, and will likely exert their own effects on the ice dynamics. Even if one uses other models to evolve the viscosity multiplier, as is common with the application of damage fields, the response time of the shear-thinning viscosity to changes in stress is instantaneous in the model, while different processes like heating and damage evolution respond over finite timescales to changes in the stress environment (Ranganathan et al., 2025; Hills et al., 2023).

Our results suggest that the impact of buttressing in ice shelves may be over-estimated in the idealized experiments designed and carried out for the $n = 3$ rheology, such as the MISMIP+ experiment and related MISOMIP experiments, designed to explore the coupling between local ocean warming and ice sheet retreat. These have generally been used to gain insight into the relative importance of buttressing and other ice-dynamic effects. The stronger stress-concentration and coincident weakening via viscosity reduction present in an $n = 4$ rheology reduce the ability of the ice shelf to maintain and transmit the stresses that provide buttressing through lateral shear stresses in $n = 3$ models. This manifest itself during the generation of a steady-state MISMIP+ initial condition for our $n = 4$ ice sheet – the reduced impact of buttressing resulted in different initial condition values than for the standard $n = 3$ experiment. Consequently, glaciologists looking for insight from benchmarks performed with $n = 3$ may also overestimate the impacts of buttressing effects in projections of real-world ice sheets.

Finally, we note that uncertainties due to the value of n compound with other uncertainties. As shown in Figure 7, the difference between $n = 3$ and $n = 4$ projections increases more than proportionally for larger forcings, implying that ice sheets which follow an $n = 4$ rheology will exhibit a greater spread between lower and upper bound response than we currently see with projections which employ $n = 3$. This functions as an uncertainty multiplier. For instance, uncertainty around time scales of ice shelf weakening ranges from the rapid disintegration of the Larsen B Ice Shelf to the more moderate (but still substantial) thinning seen in the Amundsen Sea Embayment (represented here by the ABUMIP and MISMIP+ forcing regimes). Incorporating these together, one now sees a range of more than 2× in SLR after 100 years between the n=3 moderate melt and the n=4 shelf collapse results. This finding underscores the likelihood that both the magnitude and uncertainties in current sea level rise projections are severely underestimated and that a more thorough and systematic sensitivity analysis of ice sheet models to the value of n is needed.

6 Conclusions

In this work, we show that it is possible for an $n = 3$ ice sheet model to successfully match the state of an observed $n = 4$ ice sheet, while potentially misattributing the rheology mismatch to other physics like ice damage, ice fabric, or temperature. The results of our $n = 3$ runs substantially under-predict the sensitivity and response time of ice shelves to changes in both external and internal forcings, leading to differences in both the amount and rate of grounding line retreat and contributions to sea level rise. This is likely because the viscosity multiplier is required to be fixed in time for model initialization, an algorithmic consequence not grounded in the reality of a time-dependent ice rheology.

Looking forward, it is apparent that further sensitivity studies are needed in more-realistic configurations, and projections of sea-level rise must take into account uncertainties in the viscous flow law parameters, particularly the exponent n and prefactor A, to effectively capture the range of potential responses to various forcings. Our model, like other ice-flow models used to simulate the behavior of the Antarctic Ice Sheet, strongly depends on the prescribed value of n to capture the viscous responses to stress perturbations caused by both external climate forcing and the internal variability. As such, accurately capturing the viscous stresses within glacier ice is a primary control governing our ability to predict the future of the Antarctic Ice Sheet.

Appendix A A note on the viscosity prefactor A

Ice properties represented by A_n (Equation 1) in current ice sheet models have been fitted in the context of $n = 3$ rheologies. We have no assurances that these $n = 3$ values are consistent with other values of the flow-law exponent, and in fact they are dimensionally inconsistent. To test other flow law exponents, we can exploit the fact that the viscosities $\eta_{n=3}$ and $\eta_{n=4}$ will be equal at some reference stress τ_{ref}. We can then hold viscosity constant and adjust the value of A_n in Equation 1 such that

$$\eta = \frac{\tau_{ref}^{1-n}}{2A_n} = \frac{\tau_{ref}^{1-m}}{2A_m}. \tag{A1}$$

If we assume that we know the strain rates at the particular stress $\tau = \tau_{ref}$ (equivalent to knowing the viscosity at a particular stress), then

$$A_m = A_3 \tau_{ref}^{(3-m)}, \tag{A2}$$

which provides a simple way to incorporate the temperature-dependent correlations for A developed over the past few decades (which assumed $n = 3$) to modeling ice in which $n = 4$. Conversely, if we're starting in a modeled world wherein $n = 4$, we can compute the equivalent value for A_3 using the following:

$$A_3 = A_4 \tau_{ref} \tag{A3}$$

and we can write the viscosity

$$\eta_3 = A_4^{-1} \tau_{ref} \tau^{-2} \tag{A4}$$

Following from this approach, we can see that the viscosity η_3 will be greater than η_4 for stresses greater than τ_{ref} ($\tau > \tau_{ref}$) and vice-versa (i.e., $\eta_4 < \eta_3$ for $\tau < \tau_{ref}$), as expected for a rheology less sensitive to changes in stress.

Moreover, in equation 2 above, the viscosity multiplier multiplies the viscosity in equation A4:

$$\eta_3 = \phi A_4^{-1} \tau_{ref} \tau^{-2}. \tag{A5}$$

In our idealized setup, this illustrates why neither the choice of the reference stress nor the initial rate factor should affect the ability to initialize the $n = 3$ experiment. As a product of all these factors, the inversion cannot distinguish between them.

Open Research Section

All code and relevant data and input files for this work are freely available. The numerical experiments in this work were conducted using the BISICLES open-source ice sheet model (`https://bisicles.lbl.gov`), which in turn is built upon the Chombo open-source software framework (`https://chombo.lbl.gov`) (Adams et al., 2001-2021)

Downloading Chombo and BISICLES requires free registration at `https://anag-repo.lbl.gov`, and then can be downloaded using svn. For Chombo (this work uses svn revision 23947):

```
svn --username username co https://anag-repo.lbl.gov/svn/Chombo/release/3.2
Chombo
```

For BISICLES (this work uses svn revision 4414):

```
svn --username username co https://anag-repo.lbl.gov/svn/BISICLES/public/trunk
BISICLES
```

We have placed the relevant data in a repository at the National Energy Research Scientific Computing Center (NERSC):

`https://portal.nersc.gov/cfs/m1041/dmartin/n4RheologyData`

In this location are tarfiles containing the input and data files used in this work, along with a set of README files with instructions on how to reproduce these results. For convenience, we also include the specific versions of Chombo and BISICLES used in this work in `Chombo.tar.gz` and `BISICLES.tar.gz`.

Conflict of Interest Statement

The authors have no conflicts of interest to declare. Disclosure: BM is a co-founder of Arête Glacier Initiative (areteglaciers.org), where he maintains an affiliation through his allowance for outside professional activities provided by Caltech (current affiliation) and MIT (past affiliation). Arête is a non-profit organization (currently a fiscally sponsored project of the 401(c) 3 Digital Harbor Foundation) founded in 2024 to provide funding for glaciological research focused on sea-level rise. No funding was provided by Arête for this work.

Acknowledgments
Miigwech is the word for thanks in Ojibwe. We thank Benjamin Getraer and an anonymous reviewer for their thoughtful and constructive feedback, which have substantially improved the quality and clarity of this work. We also thank a wide range of colleagues for many fruitful discussions on this and other topics. Financial support for this study was provided through the Scientific Discovery through Advanced Computing (SciDAC) program funded by the U.S. Department of Energy (DOE), Office of Science, Biological and Environmental Research and Advanced Scientific Computing Research programs, as a part of the ProSPect SciDAC Partnership. Work at Berkeley Lab was supported by the Director, Office of Science, of the U.S. Department of Energy under Contract No. DE-AC02-05CH11231. This research used resources of the National Energy Research Scientific Computing Center (NERSC), a U.S. Department of Energy Office of Science User Facility located at Lawrence Berkeley National Laboratory, operated under Contract No. DE-AC02-05CH11231 using NERSC award ASCR-ERCAPm1041. SBK was funded by DoE grant C3710, Framework for Antarctic System Science in E3SM and by the DOMINOS project, a component of the International Thwaites Glacier Collaboration (ITGC). Support from National Science Foundation (NSF: Grant 1738896) and Natural Environment Research Council (NERC: Grant NE/S006605/1). Support for BMM was also provided through funding from the Grantham Foundation. MT and SLC were supported by the Natural Environment Research Council on the ISOTIPIC project (NERC Grant NE/Y503320/1).

References

Adams, M., Colella, P., Graves, D. T., Johnson, J. N., Keen, N. D., Ligocki, T. J., … Van Straalen, B. (2001-2021). *Chombo software package for AMR applications - Design Document* (Tech. Rep. No. LBNL-6616E). Lawrence Berkeley National Laboratory. Retrieved from `https://commons.lbl.gov/display/chombo/Chombo+-+Software+for+Adaptive+Solutions+of+Partial+Differential+Equations`

Asay-Davis, X. S., Cornford, S. L., Durand, G., Galton-Fenzi, B. K., Gladstone, R. M., Gudmundsson, G. H., … Seroussi, H. (2016). Experimental design for three interrelated marine ice sheet and ocean model intercomparison projects: MISMIP v. 3 (MISMIP+), ISOMIP v. 2 (ISOMIP+) and MISOMIP v. 1 (MISOMIP1). *Geoscientific Model Development*, *9*(7), 2471–2497. doi: 10.5194/gmd-9-2471-2016

Bassis, J. N., Crawford, A., Kachuck, S. B., Benn, D. I., Walker, C., Millstein, J., … Luckman, A. (2024). Stability of ice shelves and ice cliffs in a changing climate [Journal Article]. *Annual Review of Earth and Planetary Sciences*, *52*(Volume 52, 2024), 221-247. Retrieved from `https://www.annualreviews.org/content/journals/10.1146/annurev-earth-040522-122817` doi: https://doi.org/10.1146/annurev-earth-040522-122817

Bons, P. D., Kleiner, T., Llorens, M.-G., Prior, D. J., Sachau, T., Weikusat, I., & Jansen, D. (2018). Greenland ice sheet: Higher nonlinearity of ice flow significantly reduces estimated basal motion. *Geophysical Research Letters*, *45*(13), 6542–6548.

Borstad, C., Khazendar, A., Scheuchl, B., Morlighem, M., Larour, E., & Rignot, E. (2016). A constitutive framework for predicting weakening and reduced buttressing of ice shelves based on observations of the progressive deterioration of the remnant Larsen B Ice Shelf. *Geophysical Research Letters*, *43*(5), 2027-2035. Retrieved from `https://agupubs.onlinelibrary.wiley.com/doi/abs/10.1002/2015GL067365` doi: https://doi.org/10.1002/2015GL067365

Borstad, C. P., Khazendar, A., Larour, E., Morlighem, M., Rignot, E., Schodlok, M. P., & Seroussi, H. (2012). A damage mechanics assessment of the Larsen B ice shelf prior to collapse: Toward a physically-based calving law. *Geophysical Research Letters*, *39*(18). Retrieved from `https://agupubs.onlinelibrary.wiley.com/doi/abs/10.1029/2012GL053317` doi: https://doi.org/10.1029/2012GL053317

Bromer, D., & Kingery, W. (1968). Flow of polycrystalline ice at low stresses and small strains. *Journal of Applied Physics*, *39*(3), 1688–1691.

Budd, W. F., & Jacka, T. (1989). A review of ice rheology for ice sheet modelling. *Cold regions science and technology*, *16*(2), 107–144.

Cornford, S., Martin, D., Graves, D., Ranken, D., Brocq, A. L., Gladstone, R., … Lipscomb, W. (2013). Adaptive mesh, finite volume modeling of marine ice sheets. *Journal of Computational Physics*, *232*, 529-549.

Cornford, S. L., Martin, D. F., Payne, A. J., Ng, E. G., Le Brocq, A. M., Gladstone, R. M., … Vaughan, D. G. (2015). Century-scale simulations of the response of the West Antarctic Ice Sheet to a warming climate. *The Cryosphere*, *9*(4), 1579–1600. doi: 10.5194/tc-9-1579-2015

Cornford, S. L., Seroussi, H., Asay-Davis, X. S., Gudmundsson, G. H., Arthern, R., Borstad, C., … Yu, H. (2020). Results of the third Marine Ice Sheet Model Intercomparison Project (MISMIP+). *The Cryosphere*, *14*(7), 2283–2301. doi: 10.5194/tc-14-2283-2020

Cuffey, K., & Kavanaugh, J. (2011). How nonlinear is the creep deformation of polar ice? a new field assessment. *Geology*, *39*(11), 1027–1030.

Cuffey, K. M., & Paterson, W. S. B. (2010). *The physics of glaciers.* Academic Press.

Duval, P., Ashby, M., & Anderman, I. (1983). Rate-controlling processes in the creep of polycrystalline ice. *The Journal of Physical Chemistry*, *87*(21), 4066–4074.

Dyson, F. (2004). A meeting with Enrico Fermi. *Nature*, *427*. doi: https://doi.org/10.1038/427297a

Edwards, T., Nowicki, S., Marzeion, B., & et al. (2021). Projected land ice contributions to twenty-first-century sea level rise. *Nature*, *593*, 74–82. doi: 10.1038/s41586-021-03302-y

Fan, S., Wang, T., Prior, D. J., Breithaupt, T., Hager, T. F., & Wallis, D. (2025). Flow laws for ice constrained by 70 years of laboratory experiments. *Nature*

geoscience, 1–9.
Fricker, H. A., Galton-Fenzi, B. K., Walker, C. C., Freer, B. I. D., Padman, L., & DeConto, R. (2025). Antarctica in 2025: Drivers of deep uncertainty in projected ice loss. *Science*, *387*(6734), 601–609. doi: 10.1126/science.adt9619
Gagliardini, O., Zwinger, T., Gillet-Chaulet, F., Durand, G., Favier, L., de Fleurian, B., ... Thies, J. (2013). Capabilities and performance of Elmer/Ice, a new-generation ice sheet model. *Geosci. Model Dev.*, *6*, 1299-1318. doi: doi:10.5194/gmd-6-1299-2013
Getraer, B., & Morlighem, M. (2025). Increasing the Glen–Nye power-law exponent accelerates ice-loss projections for the Amundsen Sea Embayment, West Antarctica. *Geophysical Research Letters*, *52*(7), e2024GL112516. Retrieved from `https://agupubs.onlinelibrary.wiley.com/doi/abs/10.1029/2024GL112516` (e2024GL112516 2024GL112516) doi: https://doi.org/10.1029/2024GL112516
Gillet-Chaulet, F., Hindmarsh, R. C., Corr, H. F., King, E. C., & Jenkins, A. (2011). In-situ quantification of ice rheology and direct measurement of the Raymond Effect at Summit, Greenland using a phase-sensitive radar. *Geophysical Research Letters*, *38*(24).
Glen, J. (1952). Experiments on the deformation of ice. *Journal of Glaciology*, *2*(12), 111–114.
Glen, J. W., & Perutz, M. F. (1955). The creep of polycrystalline ice. *Proceedings of the Royal Society of London. Series A. Mathematical and Physical Sciences*, *228*(1175), 519-538. Retrieved from `https://royalsocietypublishing.org/doi/abs/10.1098/rspa.1955.0066` doi: 10.1098/rspa.1955.0066
Goldsby, D., & Kohlstedt, D. L. (2001). Superplastic deformation of ice: Experimental observations. *Journal of Geophysical Research: Solid Earth*, *106*(B6), 11017–11030.
Gudmundsson, G. H. (2003). Transmission of basal variability to a glacier surface. *Journal of Geophysical Research: Solid Earth*, *108*(B5). Retrieved from `https://agupubs.onlinelibrary.wiley.com/doi/abs/10.1029/2002JB002107` doi: https://doi.org/10.1029/2002JB002107
Hills, B. H., Christianson, K., Jacobel, R. W., Conway, H., & Pettersson, R. (2023). Radar attenuation demonstrates advective cooling in the Siple Coast ice streams. *Journal of Glaciology*, *69*(275), 566–576. doi: 10.1017/jog.2022.86
Hoffman, M. J., Perego, M., Price, S. F., Lipscomb, W. H., Zhang, T., Jacobsen, D., ... Bertagna, L. (2018). MPAS-Albany Land Ice (MALI): a variable-resolution ice sheet model for earth system modeling using Voronoi grids. *Geoscientific Model Development*, *11*(9), 3747–3780. Retrieved from `https://gmd.copernicus.org/articles/11/3747/2018/` doi: 10.5194/gmd-11-3747-2018
Hudleston, P. J. (2015). Structures and fabrics in glacial ice: A review. *Journal of Structural Geology*, *81*, 1–27. doi: 10.1016/j.jsg.2015.09.003
Jezek, K. C., Alley, R. B., & Thomas, R. H. (1985). Rheology of glacier ice. *Science*, *227*(4692), 1335–1337.
Kachuck, S. B., Whitcomb, M., Bassis, J. N., Martin, D. F., & Price, S. F. (2022). Simulating ice-shelf extent using damage mechanics. *Journal of Glaciology*, *68*(271), 987–998. doi: 10.1017/jog.2022.12
Khrulev, C., Aschwanden, A., Bueler, E., Brown, J., Maxwell, D., Albrecht, T., ... Schoell, S. (2025, March). *Parallel Ice Sheet Model (PISM).* Zenodo. Retrieved from `https://doi.org/10.5281/zenodo.14991122` doi: 10.5281/zenodo.14991122
Kulp, S. A., & Strauss, B. H. (2019). New elevation data triple estimates of global vulnerability to sea-level rise and coastal flooding. *Nature Communications*, *10*(1), 4844. doi: 10.1038/s41467-019-12808-z
Larour, E., Seroussi, H., Morlighem, M., & Rignot, E. (2012). Continental scale,

high order, high spatial resolution, ice sheet modeling using the Ice Sheet System Model. *J. Geophys. Res.*, *117*. doi: doi:10.1029/2011JF002140

Lipscomb, W. H., Price, S. F., Hoffman, M. J., Leguy, G. R., Bennett, A. R., Bradley, S. L., ... Worley, P. H. (2019). Description and evaluation of the Community Ice Sheet Model (CISM) v2.1. *Geoscientific Model Development*, *12*(1), 387–424. Retrieved from https://gmd.copernicus.org/articles/12/387/2019/ doi: 10.5194/gmd-12-387-2019

MacAyeal, D. R. (1993). A tutorial on the use of control methods in ice-sheet modeling. *Journal of Glaciology*, *39*(131), 91–98. doi: 10.3189/S0022143000015744

Martin, D. F., Cornford, S. L., & Payne, A. J. (2019). Millennial-scale vulnerability of the Antarctic Ice Sheet to regional ice shelf collapse. *Geophysical Research Letters*, *46*(3), 1467-1475. Retrieved from https://agupubs.onlinelibrary.wiley.com/doi/abs/10.1029/2018GL081229 doi: https://doi.org/10.1029/2018GL081229

Millstein, J., Minchew, B., & Pegler, S. (2022). Ice viscosity is more sensitive to stress than commonly assumed. *Commun Earth Environ*, *3*(57). Retrieved from https://doi.org/10.1038/s43247-022-00385-x doi: 10.1038/s43247-022-00385-x

Minchew, B. M., Meyer, C. R., Robel, A. A., Gudmundsson, G. H., & Simons, M. (2018). Processes controlling the downstream evolution of ice rheology in glacier shear margins: case study on Rutford Ice Stream, West Antarctica. *Journal of Glaciology*, *64*(246), 583–594. doi: 10.1017/jog.2018.47

Morlighem, M. (2022). *MEaSUREs BedMachine Antarctica, version 3.* NASA National Snow and Ice Data Center Distributed Active Archive Center. Retrieved from http://nsidc.org/data/NSIDC-0756/versions/3 doi: 10.5067/FPSU0V1MWUB6

Morlighem, M., & Goldberg, D. (2023). Data assimilation in glaciology. In A. Ismail-Zadeh, F. Castelli, D. Jones, & S. Sanchez (Eds.), *Applications of data assimilation and inverse problems in the earth sciences* (p. 93–111). Cambridge University Press.

Mouginot, J., Rignot, E., & Scheuchl, B. (2019). *MEaSUREs Phase-Based Antarctica Ice Velocity Map, Version 1 [Data Set].* Retrieved 2024-01-29, from https://nsidc.org/data/nsidc-0754/versions/1 doi: 10.5067/PZ3NJ5RXRH10

Oppenheimer, M., Glavovic, B., Hinkel, J., van de Wal, R., Magnan, A., Abd-Elgawad, A., ... Sebesvari, Z. (2019). Sea level rise and implications for low-lying islands, coasts and communities. In H.-O. Pörtner et al. (Eds.), *Ipcc special report on the ocean and cryosphere in a changing climate* (pp. 321–445). Cambridge, UK and New York, NY, USA: Cambridge University Press. doi: 10.1017/9781009157964.006

Ranganathan, M., Minchew, B., Meyer, C. R., & Gudmundsson, G. H. (2021). A new approach to inferring basal drag and ice rheology in ice streams, with applications to West Antarctic ice streams. *Journal of Glaciology*, *67*(262), 229–242. doi: 10.1017/jog.2020.95

Ranganathan, M., Minchew, B., Meyer, C. R., & Peč, M. (2021). Recrystallization of ice enhances the creep and vulnerability to fracture of ice shelves. *Earth and Planetary Science Letters*, *576*, 117219. doi: 10.1016/j.epsl.2021.117219

Ranganathan, M., Robel, A. A., Huth, A., & Duddu, R. (2025). Glacier damage evolution over ice flow timescales. *The Cryosphere*, *19*(4), 1599–1619. Retrieved from https://tc.copernicus.org/articles/19/1599/2025/ doi: 10.5194/tc-19-1599-2025

Scambos, T. A., Bohlander, J. A., Shuman, C. A., & Skvarca, P. (2004). Glacier acceleration and thinning after ice shelf collapse in the Larsen B embayment, Antarctica. *Geophysical Research Letters*, *31*(18). Retrieved from https://

agupubs.onlinelibrary.wiley.com/doi/abs/10.1029/2004GL020670 doi: https://doi.org/10.1029/2004GL020670

Schohn, C. M., Iverson, N. R., Zoet, L. K., Fowler, J. R., & Morgan-Witts, N. (2025). Linear-viscous flow of temperate ice. *Science*, *387*(6730), 182-185. Retrieved from https://www.science.org/doi/abs/10.1126/science.adp7708 doi: 10.1126/science.adp7708

Schoof, C., & Hindmarsh, R. (2010). Thin-film flows with wall slip: an asymptotic analysis of higher order glacier flow models. *Q. Jl Mech. Appl. Math.*, *63*(1), 73-114.

Schulson, E. M., & Duval, P. (2009). *Creep and fracture of ice*. Cambridge: Cambridge University Press.

Sergienko, O. (2025, Jun). Pine Island Glacier ice shelf (West Antarctica) is more sensitive to climate conditions than to rheological parameters on multidecadal timescales. *Phys. Rev. E*, *111*, L062201. Retrieved from https://link.aps.org/doi/10.1103/n3xh-bt95 doi: 10.1103/n3xh-bt95

Seroussi, H., Nowicki, S., Payne, A. J., Goelzer, H., Lipscomb, W. H., Abe-Ouchi, A., ... Zwinger, T. (2020). ISMIP6 Antarctica: a multi-model ensemble of the Antarctic Ice Sheet evolution over the 21st century. *The Cryosphere*, *14*(9), 3033–3070. Retrieved from https://tc.copernicus.org/articles/14/3033/2020/ doi: 10.5194/tc-14-3033-2020

Seroussi, H., Pelle, T., Lipscomb, W. H., Abe-Ouchi, A., Albrecht, T., Alvarez-Solas, J., ... Zwinger, T. (2024). Evolution of the Antarctic Ice Sheet over the next three centuries from an ISMIP6 model ensemble. *Earth's Future*, *12*(9), e2024EF004561. Retrieved from https://agupubs.onlinelibrary.wiley.com/doi/abs/10.1029/2024EF004561 (e2024EF004561 2024EF004561) doi: https://doi.org/10.1029/2024EF004561

Steinemann, S. (1954). Results of preliminary experiments on the plasticity of ice crystals. *Journal of Glaciology*, *2*(16), 404–416.

Sun, S., Pattyn, F., Simon, E. G., Albrecht, T., Cornford, S., Calov, R., ... et al. (2020). Antarctic Ice Sheet response to sudden and sustained ice-shelf collapse (ABUMIP). *Journal of Glaciology*, *66*(260), 891–904. doi: 10.1017/jog.2020.67

Tsai, V. C., Stewart, A. L., & Thompson, A. F. (2015). Marine ice-sheet profiles and stability under coulomb basal conditions. *Journal of Glaciology*, *61*(226), 205–215. doi: 10.3189/2015JoG14J221

Turcotte, D., & Schubert, G. (2014). *Geodynamics* (3rd ed.). Cambridge University Press.

Wang, Y., Lai, C.-Y., Prior, D. J., & Cowen-Breen, C. (2025). Deep learning the flow law of Antarctic ice shelves. *Science*, *387*(6739), 1219-1224. Retrieved from https://www.science.org/doi/abs/10.1126/science.adp3300 doi: 10.1126/science.adp3300